Inhibition of APOC1 promotes the transformation of M2 into M1 macrophages via the ferroptosis pathway and enhances *anti*-PD1 immunotherapy in hepatocellular carcinoma based on single-cell RNA sequencing

Xiaopei Hao [a,1], Zhiying Zheng [b,1], Hanyuan Liu [c,1], Yao Zhang [a,1], Junwei Kang [b], Xiangyi Kong [a], Dawei Rong [a], Guangshun Sun [c], Guoqiang Sun [c], Li Liu [d,e,****], Haibo Yu [f,***], Weiwei Tang [a,**], Xuehao Wang [a,*]

[a] *Hepatobiliary Center, The First Affiliated Hospital of Nanjing Medical University, Key Laboratory of Liver Transplantation, Chinese Academy of Medical Sciences, NHC Key Laboratory of Living Donor Liver Transplantation, Nanjing, China*
[b] *Department of Anesthesiology, The First Affiliated Hospital of Nanjing Medical University, Nanjing, China*
[c] *Department of General Surgery, Nanjing First Hospital, Nanjing Medical University, Nanjing, China*
[d] *First Teaching Hospital of Tianjin University of Traditional Chinese Medicine, Tianjin, China*
[e] *State Key Laboratory of Modern Chinese Medicine, Tianjin University of Traditional Chinese Medicine, Tianjin, China*
[f] *Department of Hepatobiliary Surgery, People's Hospital of Zhengzhou University, Zhengzhou, China*

ARTICLE INFO

ABSTRACT

Single-cell RNA-sequencing (scRNA-seq) presents better insights into cell behavior in the context of a complex tumor microenvironment by profiling single-cell populations. However, the mechanisms underlying treatment failure in hepatocellular carcinoma (HCC) are poorly understood. In this study, we performed deep scRNA-seq on immune cells under the isolation in peripheral blood, cancer tissues, and nearby common tissues of four HCC cases and two non-cancer controls, and 212,494 cells were included in the analysis. We identified distinct immune cell subtypes, enriched pathways for differential genes, and delineated associated developmentally relevant trajectories. APOC1 was found over-expressed in tumor-associated macrophages (TAMs) of HCC tissues than in normal tissues. Inhibition of APOC1 reversed the M2 phenotype to the M1 phenotype via the ferroptosis pathway in TAMs from HCC. Tumors in APOC1 $^{-/-}$ C57BL/6 mice demonstrated consistent attenuation compared to wild-type (WT) mice. Mass spectrometry results revealed that the relative proportion of M2 macrophages, B cells, and CD4$^+$ T cells in the APOC1 $^{-/-}$ group exhibited a downward expression compared with the WT group, whereas CD8$^+$ T cells, M1 macrophages, and NK cells exhibited an upward trend. Finally, APOC1 was found to be negatively correlated with the expression of PD1/PD-L1 in human HCC samples. In conclusion, the present study demonstrated that inhibiting APOC1 can promote the transformation of M2 macrophages into M1 macrophages via the ferroptosis pathway, thereby reshaping the tumor immune microenvironment and improving the *anti*-PD1 immunotherapy for HCC, providing a new strategy for improving the therapeutic effect of *anti*-PD1, and bringing new hope to HCC patients.

* Corresponding author.
** Corresponding author.
*** Corresponding author.
**** Corresponding author.
E-mail addresses: jewtou@gmail.com (L. Liu), yhb2101661@163.com (H. Yu), 1243773473twww@sina.com (W. Tang), wangxh@njmu.edu.cn (X. Wang).
[1] These authors contributed equally to this work.

1. Introduction

Liver malignancies are one of the most prevalent solid tumors and the second leading cause of cancer-related deaths worldwide, with an estimated 830,180 new deaths in 2020 [1]. Hepatocellular carcinoma (HCC) is the most prevalent primary liver cancer worldwide, and its incidence is rising globally. HCC is associated with chronic hepatitis virus infection, long-term exposure to carcinogens such as aflatoxins, excessive alcohol consumption, nonalcoholic fatty liver disease, hemochromatosis, and alpha-1 antitrypsin deficiency [2]. At the time of diagnosis, most HCC patients are at an advanced stage, and surgical treatment may not be effective. According to statistics, the five-year survival rate following liver cancer surgery is only 10%–18% [3]. Recently, several new treatments have emerged, such as transcatheter arterial chemoembolization (TACE) and radiofrequency ablation (RFA), which can effectively treat local lesions but cannot completely eradicate residual cancer cells, leading to tumor recurrence and metastasis. This dilemma is being resolved by molecular targeted therapy. Targeted drugs can inhibit cancer cells through cell signaling pathways, proto-oncogenes, tumor suppressor genes, and cytokines. Sorafenib, the first liver-targeted drug approved by the Food and Drug Administration (FDA), has been widely used in clinical practice. With the advent of targeted drugs, patient survival has improved dramatically [4]. Molecular targeted drugs with higher selectivity, sensitivity, and effectiveness have become the first-line drugs for HCC treatment. However, the problems of targeted therapy, such as severe side effects, low survival rate, and drug resistance, have yet to be resolved [5].

With a series of advances in tumor immunotherapy, the immunotherapy of HCC has received increasing attention. The importance of the tumor microenvironment (TME) in HCC development has been established. TME is a dynamic system composed of cancer cells, cytokines, extracellular matrix, and immune cell subpopulations. Immunotherapy inhibits tumor progression by altering the tumor microenvironment. Immunotherapy-related targets, such as programmed death-1 receptor (PD1), programmed death-1 receptor ligand (PD-L1), and CD8$^+$ tumor-infiltrating cells (TILs), are widely expressed in the HCC tumor microenvironment [6]. These targets provide favorable immunotherapeutic conditions for HCC. HCC immunotherapy mainly includes immune checkpoint inhibitors (ICIs), cytokine therapy, tumor vaccine, and immune cell therapy. Various current clinical trials represented by ICIs have provided growing medical evidence for the clinical application of HCC immunotherapy. Common immune checkpoints include cytotoxic T lymphocyte-associated antigen 4 (CTLA-4), PD1, PD-L1, T cell immunoglobin 3 (TIM3), and lymphocyte-activation gene 3 (LAG3) [7]. Nivolumab, the first PD1 monoclonal antibody, was approved by the FDA in September 2017 for the second-line treatment of advanced HCC. A phase II clinical trial (CHECKMATE 040) involving 262 patients with advanced HCC demonstrated an overall objective response rate of 20% and disease control rate of 64% in patients with advanced HCC treated with nivolumab [8]. The results of phase III clinical trial (CHECKMATE 459) involving 743 HCC patients who had not received systemic treatment demonstrated that nivolumab had a longer disease control duration (median disease control duration 7.5 vs. 5.7 months), better safety, and fewer treatment-related adverse events (22% vs. 49%) compared to sorafenib [9]. Subsequently, a variety of PD1 monoclonal antibodies were introduced for HCC treatment, and all of them proved that immune checkpoint inhibitors targeting PD1 had development prospects in the treatment of HCC through clinical trials, establishing the first therapy with a survival rate better than sorafenib, which is a milestone significance in HCC treatment [10].

Single-cell RNA sequencing (scRNA-seq) is a new technique for transcriptome analysis of single cells. The sensitivity, accuracy, and efficiency of scRNA-seq have increased over the past decade with the advent of more sensitive, automated, and cost-effective single-cell separation methods, as well as innovations in high-throughput technologies and improved operational processes. scRNA-seq can provide greater insight into the biological behavior of cells in complex tumor microenvironments, especially through the analysis of single-cell populations [11]. The pathogenesis and therapeutic principles of HCC remain unclear, and numerous studies have demonstrated a variety of heterogeneous cells in the tumor microenvironment with HCC. scRNA-seq enables a comprehensive understanding of the pathogenesis of HCC. In the present study, we used scRNA-seq analysis to explore the function and transcriptional characteristics of CD45$^+$ cells in eight HCC samples and focused on different analyses of immune cells in both tissues and peripheral blood. We identified different immune cell subtypes covering macrophage, natural killer cell (NK), B lymphocyte, CD8 T lymphocyte, and CD4 T lymphocyte, and delineated their developmental trajectories as well as analyzed enrichment pathways. We found that APOC1 was enriched in TAMs of HCC tissues. Borgquist et al. [12] reported that circulating APOC1 levels in humans are associated with cancer risk. Jie Yi et al. [13] demonstrated that APOC1 expression was significantly higher in gastric cancer (GC) tissues than in adjacent non-cancer tissues. APOC1 expression was correlated with clinical stage, tumor classification, and lymph node metastasis. APOC1 may be a potential serum biomarker for GC diagnosis. Several studies have demonstrated that APOC1 is involved in the progression and development of various cancers, such as colorectal cancer (CRC), prostate cancer (PCa), lung cancer, pancreatic cancer, kidney cancer, etc. [14–17]. Our study found that inhibition of APOC1 can promote the transformation of M2 macrophages into M1 macrophages via the ferroptosis pathway, reshaping the tumor immune microenvironment and improving *anti*-PD1 immunotherapy for HCC.

2. Materials and methods

2.1. Ethics statement

According to the Ethics Committee of the First Affiliated Hospital of Nanjing Medical University, the protocol here received a review and gained approval. The respective case provided the informed consent in a written form regarding samples' experiments-related application. Furthermore, this study adhered to all applicable guidelines and regulations.

2.2. Patients and specimens

Samples were obtained from the Liver Transplanting Center, the First Affiliated Hospital of Nanjing Medical University. Samples of carcinoma tissues were derived from two HCC cases carrying non-metastasis, major, non-treated carcinomas receiving HCC resecting. The adjacent normal tissues received the taking from over 5 cm in cancerous tissues' negative margins. Two HCC cases provided peripherally samples of blood in advance of surgery. Two peripheral blood samples were taken from two non-cancer controls and were obtained from the individuals in the physically-related examining station of the First Affiliated Hospital of Nanjing Medical University abiding by the Helsinki Declaration.

2.2.1. scRNA-seq analysis

Raw counts obtained from Illumina Hiseq4000 sequencer (Capital-Bio, Beijing, China) were aligned to the Human reference (GRCh38 version), provided by 10x Genomics company, using the 10x Genomics CellRanger pipeline (version 2.1.0). The filtered expression matrix generated by CellRanger for each sample was analyzed and processed with the R package Seurat. Quality control of the single-cell expression matrix was also performed using Seurat (version 3.2.0). Cells were first filtered for quality based on the following criteria: having a unique molecular identifier (UMI) count above 500, mapping to over 100 unique genes, and the fraction of unique mitochondrial transcripts was less than 15%. Doublets in the cells were detected using the R package Doublet Finder with default parameters. Supposed doublets were dropped, and the remained cells from all samples were merged with

Seurat for further analysis.

2.3. Cell cluster analysis

The merged expression matrix was normalized and scaled with library size, and the percentage of mitochondrial reads regressed with Seurat. In total, 2000 highly variable genes (hvg) were calculated using Find Variable Features from Seurat and then used in the principal component analysis (PCA) with parameter npcs = 30. Based on the PCA result, the Harmony program (version 0.1.0) was used to remove potential batches among samples with parameter npca = 12. After correcting batches with Harmony, a new dimensionality reduction named harmony was produced in Seurat single-cell object. The harmony dimensionality reduction, instead of PCA dimensionality reduction, was used to construct a shared nearest neighbor graph by calculating the neighborhood overlap (Jaccard index) between every cell in the scRNA dataset using FindNeighbors from Seurat. The shared nearest neighbor graph was then used to identify clusters of cells using FindClusters from Seurat. T-Distributed stochastic neighbor embedding (tSNE) dimensionality reduction and Uniform Manifold Approximation and Projection (UMAP) dimensionality reduction were performed on the harmony dimensionality reduction for visualization using RunTSNE and RunUMAP from Seurat.

We tested a wide range of resolutions, and the output numbers of identified cell clusters varied with different resolution parameters. To choose a proper resolution parameter, the ROGUE method was used to evaluate the purity of output clusters and select the most optimized resolution parameter. After clustering cells with selected resolution parameters, the Wilcoxon rank sum test was performed to identify upregulated genes in each cluster using the FindAllMarkers function from Seurat. We found that some clusters might share quite similar marker genes. We also checked the cell distribution on tSNE or UMAP. If two clusters were located close to each other on tSNE or UMAP and also shared quite similar marker genes at the same time, the clusters would be considered the same cell type and manually merged into a single cluster.

The Wilcoxon rank sum test was performed again to identify significantly upregulated genes in each manually modified cluster using FindAllMarkers. The significantly upregulated genes were used to infer cell types.

2.4. Monocle trajectory analysis

Monocle (Version 2.18.0) was used to infer the developmental trajectories of monocyte and macrophage cells. All monocytes and macrophages were separated from the Seurat object, transferred into SingleCellExperiment format, and then applied for trajectory analysis with monocle following the official tutorial (http://cole-trapnell-lab.github.io/monocle-release/docs/#constructing-single-cell-trajectories). The Monocle object was constructed from the SingleCellExperiment format using the new Cell Data Set function in Monocle. The Estimate Size Factors function was used to estimate the size factors for all cells, and then the Dispersions were used to estimate the dispersions for all genes. The genes with mean expression above 0.1 and expressed in more than ten cells were selected and applied for differential expression statistical test using differential Gene Test among different monocyte and macrophage sub-cell types. Differentially expressed genes with qval lower than 0.01 were used to order cells and generate pseudotime trajectories.

2.5. Cancer cell culture

The Cell Bank of Type Culture Collection (Chinese Academy of Sciences, China) offered mice H22-HCC cells, human HCC cells (Hep3B and HCCLM3), cultured with RPMI 1640 medium (BI, USA) supplemented by 10% fetal bovine serum (FBS) (Gibco, USA) at 37 °C in a 5% CO_2 chamber. The maintenance was conducted on overall cell lines at 37 °C within one constant-temperature incubator with 5% CO_2.

2.6. Primary culture of THP-1 and cell transfection

THP-1 cells were cultured with RPMI 1640 medium (BI, USA) supplemented by 10% fetal bovine serum (FBS) (Gibco, USA). After the transfection of lentiviral vectors, including sh-NC and sh-APOC1 (Genechem, China) into THP-1 cells, stably transduced cells were selected using puromycin and validated using Western blot (Table S1). Cells were harvested after two days of PMA-mediated macrophage differentiation. In TAM stimulation experiments, THP-1 cells were treated with Hep3B/HCCLM3 culture supernatant in RPMI 1640 medium for two days, producing TAMs.

2.7. Cell proliferation assay

For the CCK8 assay, cancer cells were treated with supernatant derived from TAMs with sh-NC or sh-APOC1. Then, cancer cells were seeded in 96 wells and then administrated with 10 μl of CCK8 solution (Ribobio, China) when cultured at 0, 24, 48, 72, 96, and 120 h, separately. After 2 h of incubation, the absorbance value was detected with a spectrophotometer (Thermo Scientific, Pittsburgh, PA, USA) at 450 nm.

For EDU assay, Hep3B and HCCLM3 cells were treated with supernatant derived from TAMs with sh-NC or sh-APOC1. The HCC cells were used in the following experiments. Using Cell-Light EDU DNA Cell Proliferation Kit (RiboBio, China), we performed the 5-ethynyl-2′-deoxyuridine (EDU) experiment to assess cell proliferation. Cells (5×10^4/well) were seeded into 24-well plates and cultured for 24 h. The cell lines were fixed with 4% paraformaldehyde after incubating with EdU for 2 h. The rest steps were performed according to the manufacturer's protocol. EdU cell lines were captured and counted under an Olympus FSX100 microscope (Olympus, Japan).

2.8. Transwell invasion assay

Hep3B and HCCLM3 cells were treated with supernatant derived from TAMs with sh-NC or sh-APOC1. Hep3B and HCCLM3 cells then underwent the seeding process in upper chambers with 200 μl of serum-free RPMI 1640 medium. The transwell chamber (Corning, USA) was paved with matrigel mix (BD Biosciences, USA) to achieve invasion assay. RPMI 1640 medium and 10% FBS were introduced to the bottom chamber as an HCC cell chemoattractant. After being incubated for 24 h, the upper chambers underwent the fixing process and then the staining process using crystal violet (Kaigen, China) for 15 min. To achieve the visualizing process, the cell lines underwent the photographing and counting process in three fields.

2.9. Scratch wound experiment

Under the cell confluence reaching about 90% at 24 and 48 h post-transfecting process, the monolayers were scratched by a 200 μl pipette, and the cell debris was removed by washing with PBS. Medium received the addition, and the culturing plates underwent incubation at 37 °C. Wound healing received the survey at various points. Furthermore, representing scrape lines were captured.

2.10. Quantitative reverse transcription polymerase reaction (qRT-PCR)

According to the producer's protocol, total RNAs from TAM cells received the isolation based on the TRIzol reagent (Invitrogen, USA). Based on a reverse transcription kit (Takara, Japan), cDNA received the synthesis for mRNA. GAPDH was used to normalize the mRNA expressing level levels. All primer sequences are listed in Table S2.

2.11. Western blotting

Proteins were extracted using RIPA buffer (Sigma-Aldrich, USA) containing protease inhibitors. Protein lysates were separated using 10% sodium dodecyl sulfate-polyacrylamide gels (SDS-PAGE) and subsequently transferred onto polyvinylidene fluoride membranes. The primary antibodies (Abcam, UK) against APOC1, NRF2, SLC7A11, and GPX4 were used. Peroxidase-conjugated secondary antibody (CST, Sigma-Aldrich, USA) was used, and the antigen-antibody reaction was visualized by enhanced chemiluminescence assay (ECL; Thermo Fisher, USA).

2.12. Iron and ROS assay

The total iron levels in TAMs were determined using the Iron Assay Kit according to the manufacturer's instructions. In brief, cells were rapidly homogenized in iron assay buffer and centrifuge at $16,000 \times g$ for 10 min at 4 °C to remove insoluble material. Approximately 50 μl samples were added to a 96-well plate and brought the volume to 100 μl with a 50 μl assay buffer. Approximately 5 μl of Iron assay buffer or iron reducer were then added for ferrous iron or total iron measurement, respectively. After mixing and incubating in the dark for 30 min at 25 °C, 100 μl iron probes were added to each well and incubated in the dark for 60 min at 25 °C. Finally, the absorbance was measured at 550 nm, and a standard curve line was used for iron concentration calculation. Intracellular ROS amounts were determined by incubating cells for 10 min at 37 °C with the redox-sensitive probe 2'-7'-Dichlorodihydrofluorescein diacetate (CM-H2DCFDA; Thermo Fisher Scientific, USA), according to the instructions of the manufacturer.

2.13. Immunohistochemistry

The deparaffinized and rehydrating processes were conducted for sections with paraffin embedment. Hydrogen peroxide (3%) was used to block peroxidase activity. Sections were incubated throughout the night with primary antibodies purchased all from Abcam (CD3, CD8, Ki67, PD1, and PD-L1) at 4 °C. The biotinylated secondary antibody was then adopted to treat tissue sections and incubated with streptavidin-horseradish peroxidase complex (Santa Cruz Biotechnology Inc., USA).

2.14. Mice model

The animal management committee of Nanjing Medical University approved the animal experiment, and all experimental procedures and animal caring abided by the institutional ethics directions for animals-related experimental processes. The injection of H22 cells was made into mice (n = 5 in each group). Carcinoma transplanted tumor model mice were divided into four groups: wild type (WT), APOC1$^{-/-}$, αPD1, APOC1$^{-/-}$+αPD1 group, (n = 5 per group). The four groups of mice were treated by complying with the corresponding groups. αPD1 or APOC1$^{-/-}$+αPD1 group received 200 μg αPD1(Bioxcell, USA) intraperitoneal injection for seven days and twice a week after that. The activity, spirit, and diet of mice were observed daily before and after the experiment. The long diameter A (mm) and short diameter B (mm) of the tumor were determined by vernier calipers every four days, and the tumor volume (V) of the mice was calculated by $V = AB^2/2$, and the tumor growth curve was plotted. After 21 days, the mice were sacrificed by neck dissection.

2.15. Mass spectrometry

The tissue samples originated from tumors isolated from APOC1$^{-/-}$ and WT C57BL/6 mice, respectively. The mouse tissue processing method, referred to as Miltenyi Mouse Tumor Dissociation Kit, Percoll removes impurities and splits red. CyTOF staining steps consisted of 194 Pt staining → Fc block → surface antibody staining → overnight DNA staining (191/193Ir) → intracellular antibody staining → collecting data on the computer.

2.16. Statistical analysis

GraphPad Prism 8.0 (GraphPad, USA) was used for statistical analysis, and a P-value <0.05 was considered statistically significant. We performed an independent *t*-test for continuous variable comparisons among two groups and a one-way ANOVA for comparisons between multiple groups.

Results

3.1. Results acquisition of scRNA-seq profiles of samples and data generation in HCC

To analyze immune cells associated with the occurrence and progression of HCC, we carried out scRNA-seq on CD45$^+$ cells under the isolation in eight specimens covering two peripherally specimens (BH) in two cases with non-cancer, two preoperation-related peripherally blood specimens (BP) in two HCC cases, as well as two pairs of HCC tissues (T) and the relevant nearby non-cancer tissues (N) in two HCC cases. To capture cancer cell compositions' overall spectra, we sorted one subdivided cell set without selecting the process in advance under the CD45 isolating process to ensure the analyzing process of considerable immunity-related cells. Table S3 elucidated the data under the separation in terms of the respective sample, and 212,494 cells were included in the analysis. The UMAP plot demonstrated that nine common immune cell clusters were named according to marker identification and merger (Fig. 1A–C). For example, the TAM cell cluster mainly expressed C1QC, CD163, and APOC1, the NK cell cluster mainly expressed GNLY, NKG7, and GZMB, and the CD8 T cell cluster mainly expressed CD8A, CD8B, and GZMB (Fig. 1B–C). As displayed in Fig. 1D–E, histograms and heatmap indicate the specific expression of each cell cluster in different samples. For example, the expression of TAM in cancer tissues was significantly higher than that in adjacent normal tissues, but there was almost no expression in peripheral blood between BP and BH. The expression of CD8 T and NK cells in cancer tissues was lower than that in adjacent tissues, and they were also expressed in peripheral blood, but the difference was insignificant.

3.2. Analysis of T and NK cell trajectories and pathway enrichment in HCC

To reveal the transition process of the cells from childhood to exhaustion, we used the monocle R package to perform a pseudo-chronological analysis on the clusters of T cell and NK cell clusters. For T cells, seven CD8 and two CD4 cell clusters were defined in detail (Fig. 2A). Trajectory plot results demonstrated that clusters of naive CD8 T cells aggregated at the initial stage at the right end of the branch, then differentiated and matured into cytotoxic CD8 T cells, and finally exhausted CD8 T cells (Fig. 2A). As demonstrated in Fig. 2B, the CD8-S100A8 cell cluster was mainly enriched in the initial state of differentiation, CD8-GNLY, CD8-NR4A2, CD8-PDCD1, CD8-LMNA, CD8$^-$CD83 cell clusters were in the middle differentiation stage, and CD8-PDCD1 and CD8-APOA2 cell cluster was enriched in the end stage of differentiation. For CD4 T cells, CD4-TCF7 was mainly concentrated in the early stage of CD4 T cell differentiation, while CD4-FOXP3 (Treg) was mainly enriched in the middle stage of differentiation (Fig. 2B). In addition, we simulated the trajectory of three typical genes (HSPA1A, PDCD1, TCF7) and found that HSPA1A and PDCD1 expressed higher with the T cell differentiation process, while TCF7 was only expressed in the early stage of T cell differentiation (Fig. 2C). Pathway analysis demonstrated that the different genes in T cell clusters were involved in low-density lipoprotein (LDL) modeling and high-density lipoprotein (HDL) clearance, indicating that genes regulating CD8 T cells were highly correlated with
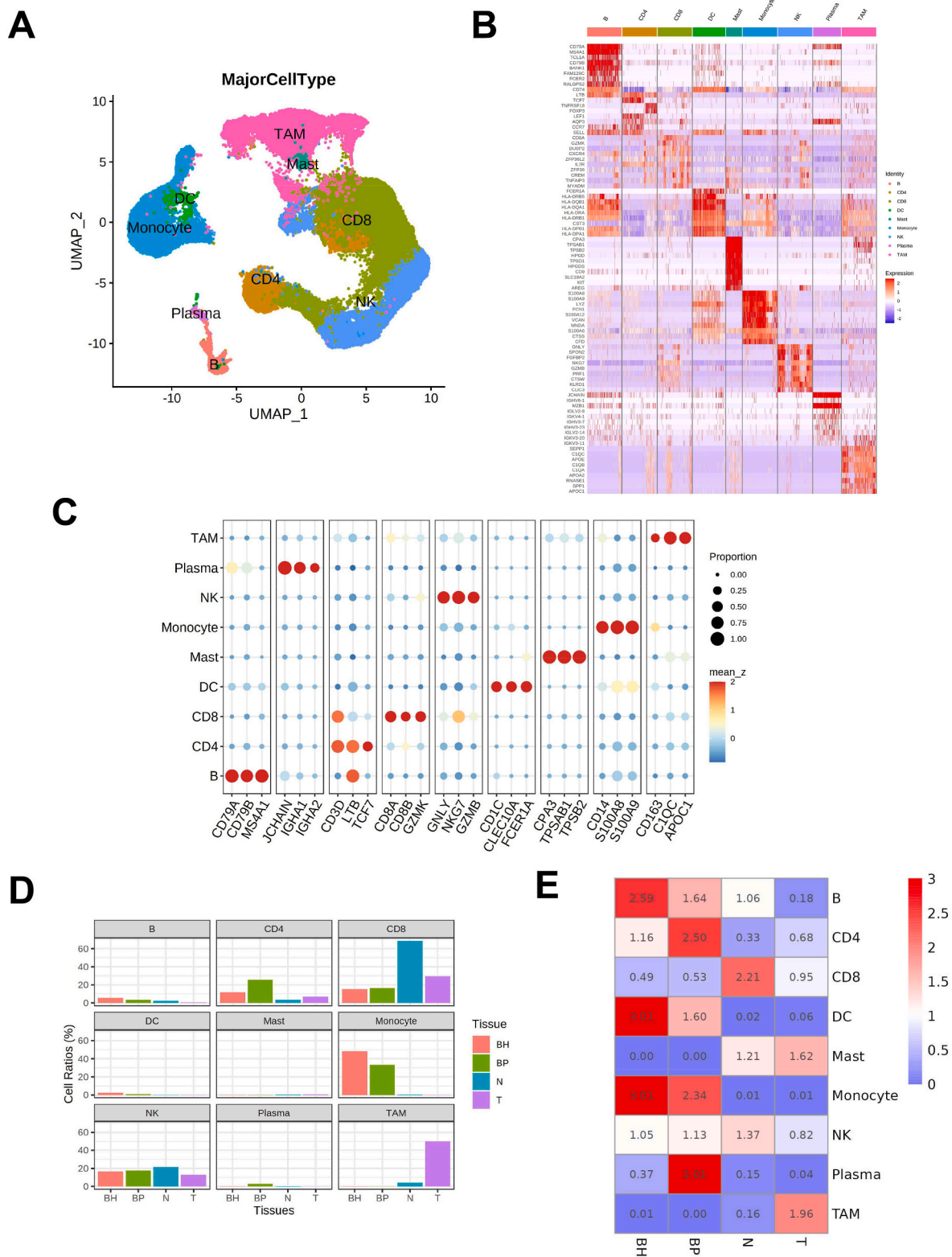
Fig. 1. Acquisition of scRNA-seq profiles of samples and data generation in HCC. (A) UMAP showing different immune cell populations which have been identified. (B) Heat maps showing markers of different cell populations. (C) Dot plots showing markers of different cell populations. (D)The bar chart showing the differences in expression of different cell populations in different samples. (E) Specific values of expression of different cell populations in different samples were presented.

lipid metabolism (Fig. 2D). In NK cell clusters, NK-CREM and NK-HSPA1B cell clusters gathered at the end of the trajectory, while NK-FGFBP2 accumulated at the beginning (Figures S1A-1B). We simulated the trajectory of three typical genes (HAVCR2, HSPA1A, IFGN) and found that these genes expressed higher with the NK cell differentiation process (Figure S1C). Pathway analysis demonstrated that NK-CREM, NK-FGFBP2, and NK-HSPA1B cell clusters were linked with hepoxilin and trioxilin syntheses (Figure S1D).
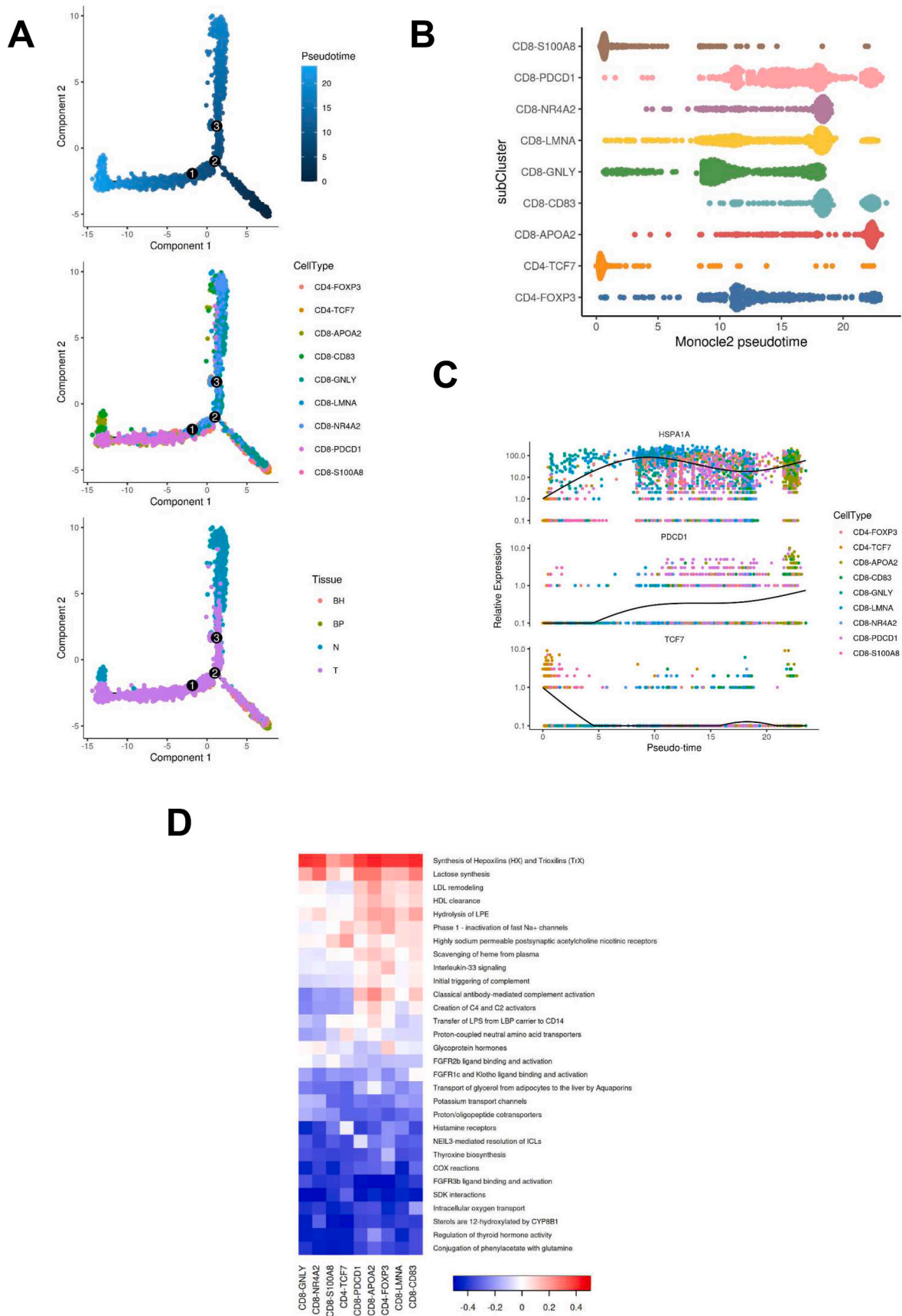
Fig. 2. Analysis of T cell trajectories and pathway enrichment in HCC. (A) The trajectory distribution of each T cell population over time in different samples. On the right is the starting point of development and on the left is the developmental endpoint. (B) The ordering of T cells along pseudotime in a two-dimensional state-space defined by Monocle 2. (C) The trajectory of three typical genes (HSPA1A, PDCD1, TCF7). (D)Pathway analysis of T cell cluster.

3.3. Detailed classification and trajectories of myeloid cell cluster in HCC

In this study, we focused on analyzing myeloid cells and analyzed the different cell clusters of myeloid cells in detail. UMAP plot revealed that five cell clusters (Mono-LST1, Mono-S100A8, TAM-APOC1, TAM-CCL5, TAM-FCN3) were named according to marker identification and merger (Fig. 3A–C and S2A-2B). For example, the Mono-LST1 cell cluster mainly expressed LST1, COTL1, and LILRB1, TAM-APOC1 cell cluster mainly expressed APOC1, FABP1, and C1QC, and TAM-FCN3 cell cluster mainly expressed FCN2, FCN3, and CCL14 (Fig. 3B–C and S2A-2B). Pseudo-chronological analysis indicated that the middle and late stages of myeloid cell differentiation mainly included TAM-APOC1, TAM-CCL5, and TAM-FCN3 cell clusters were mainly enriched in tumor tissues (Fig. 3D–E). Mono-LST1 and Mono-S100A8 were enriched in the peripheral blood and were in the early stages of myeloid cell differentiation. Furthermore, we simulated the trajectory of three typical genes (APOC1, CD14, CD163) and found that APOC1 and CD163 were generated at the middle stage of myeloid cell differentiation. Over time, APOC1 expression decreased while CD163 expression increased. CD14 was produced at the early stage of myeloid cell differentiation and tended to decline over time (Fig. 3F).

3.4. APOC1 was over-expressed in TAMs of HCC tissues based on scRNA-seq results

Based on the scRNA-seq results, we found that APOC1 may play an important role in the TAMs of HCC. Therefore, we analyzed the detailed expression of APOC1 in each sample and each cell cluster in detail. APOC1 was highly enriched in TAMs in the overall cell cluster analysis, partially expressed in mast cells, and less expressed in other cell clusters such as CD8 T, CD4 T, and NK cells (Figure S3A). Analysis between samples demonstrated that the overall expression of APOC1 in cancer tissues was significantly higher than that in adjacent cancer tissues, while the expression in peripheral blood was very low (Figure S3B). Further, different subgroup analyses of different samples suggested that the expression of APOC1 in the TAM cell cluster in HCC cancer tissues was significantly higher than that in adjacent cancer tissues (Figure S3C). The UMAP map more intuitively demonstrated the enrichment of APOC1 in different cell clusters in different samples (Figure S3D). These results aroused our great curiosity to explore the role of APOC1 in TAMs from HCC.

3.5. Inhibition of APOC1 of TAMs reduced HCC progression in vitro and in vivo

To further verify the role of APOC1 in TAMs from HCC in vitro, Western blot confirmed that APOC1 was indeed knocked down in TAMs (Fig. 4A). We stimulated HCC cells with TAM supernatant and found that TAMs in the sh-APOC1 group significantly reduced the proliferation, invasion, and migration of HCC cells compared with the control group by CCK8, EDU, transwell, and scratch assay (Fig. 4B–E). To address the possible effect exerted by APOC1 on the tumor in vivo, we injected H22 cells in WT and APOC1$^{-/-}$ C57BL/6 mice, respectively. H22 cells tended to grow in WT mice, whereas they demonstrated consistent attenuation in APOC1$^{-/-}$ mice (Fig. 4F). When the mice were sacrificed on day 21, the volume and weight of the tumor in APOC1$^{-/-}$ mice were found to be significantly smaller than those in WT C57BL/6 mice (Fig. 4G–H).

3.6. Inhibition of APOC1 reversed the M2 phenotype to the M1 phenotype via the ferroptosis pathway in TAMs from HCC

How does the reduction of APOC1 inhibit HCC? We stimulated THP-1 cells with supernatant of HCC cancer cells and detected the expression of TAM-related genes by qRT-PCR after co-cultured with sh-NC/sh-APOC1. We noticed that CD86 expression of M1 phenotype in the sh-

APOC1 group was significantly higher than that in the control group after the addition of HCC supernatant to TAM cells, whereas the expression of CD206, CD163, and ARG1 of M2 phenotype was significantly lower than that in the control group (Fig. 5A). These findings suggest that inhibition of APOC1 reversed the M2 phenotype to M1 phenotype in TAM from HCC, thereby inhibiting the growth of HCC cancer cells.

Therefore, how APOC1 transforms TAM phenotype is an interesting scientific question worthy of further exploration. We analyzed the differential genes in the TAM-APOC1 cell cluster and found that SPP1, APOA1, and APOA2 were significantly up-regulated, whereas S100A8, EMP3, and CCL5 were down-regulated (Fig. 5B). KEGG pathway analysis revealed that these different down-regulated genes were involved in the T cell receptor signaling pathway (Fig. 5C), whereas up-regulated genes were enriched in the PPAR pathway, ferroptosis, and phagosome (Fig. 5D). GSEA enrichment also confirmed that differentially expressed genes in the TAM-APOC1 cluster were involved in the ferroptosis pathway (Fig. 5E). Iron is a significant element that participates in activities such as cell proliferation, metabolism, and differentiation. Iron can determine macrophages' fate and function, especially cell development and differentiation. Studies have proved that iron overload can increase the level of M1 markers and decrease M2 makers; in other words, promoting polarization of M1 macrophages [18]. In addition to inducing inflammatory factors, iron overload aggravates atherosclerosis development by enhancing glycolysis to prompt the M1 phenotype [19]. Besides, ROS production and p53 acetylation caused by iron overload also contribute to M1 polarization [20]. However, iron overload doesn't always cause M1 polarization. Research in 2020 revealed that under chronic iron overload, THP-1 monocyte-derived macrophages tend to exhibit signs of M2 type and downregulate the markers of M1 macrophages [21]. Besides, ROS production caused by iron overload also contributes to M1 polarization [20]. To confirm that APOC1 was indeed associated with ferroptosis in TAMs, we first examined the iron content in TAMs of sh-NC and sh-APOC1 groups. The results demonstrated that iron content in the sh-APOC1 group was higher than that in the sh-NC group (Fig. 5F). The ROS probe suggested that the ROS content in the sh-APOC1 group was significantly higher than in the control group (Fig. 5G). Western blot confirmed that ferroptosis-related proteins, including GPX4, NRF2, and SLC7A11 proteins were all down-regulated in sh-APOC1 group, indicating ferroptosis increased (Fig. 5H). Electron micrographs demonstrated that the TAM mitochondria of sh-APOC1 group were pyknotic, smaller in size, higher in electron density, and expanded in cristae, consistent with the characteristics of ferroptosis (Fig. 5I). These results suggested that inhibition of APOC1 reversed the M2 phenotype into the M1 phenotype via the ferroptosis pathway in TAM from HCC, thereby inhibiting the development of HCC cancer cells.

3.7. APOC1 deficiency resulted in immune activation based on mass spectrometry analysis and enhanced sensitivity to anti-PD1 therapy in HCC

The aforementioned results proved the mechanism of APOC1 in TAMs, so the impact of APOC1 deficiency on the overall TAMs is worth further exploring. Two tumor samples from WT and APOC1$^{-/-}$ mice were detected by mass spectrometry. We cycled single, live, and intact CD45$^+$ immune cells from the selected cells in the respective tissues (Figure S4). All samples indicated clustering and subgroup annotation of CD45$^+$ immune cells. There were 33 cell clusters in total, and the respective cell clusters were defined based on the specific markers of the respective cell types (Fig. 6A–B and S5). The results indicated that the relative proportion of M2 macrophages, B cells, and CD4 T cells in the APOC1$^{-/-}$ group exhibited a downward trend than the WT group, whereas CD8 T cells, M1 macrophages, and NK cells exhibited an increasing trend (Fig. 6B–C). The expressions of PD-L1, PD1, TIGIT, TIM3, and IFNg increased in APOC1$^{-/-}$ mice (Fig. 6D–I). These results confirmed that APOC1 deficiency results in immune activation of HCC.
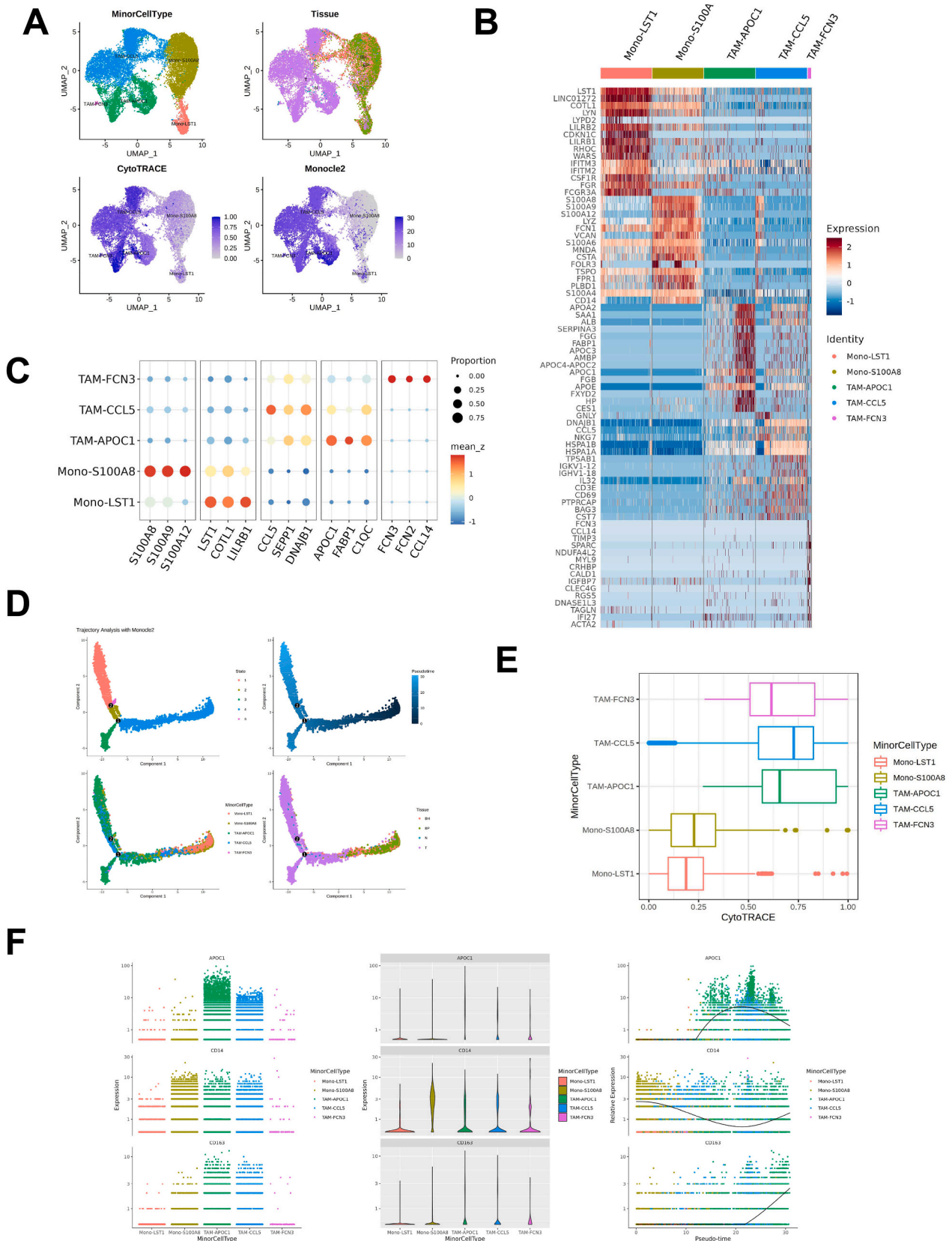
Fig. 3. Detailed classification and trajectories of myeloid cell cluster in HCC. (A) UMAP showing different myeloid cell populations which have been identified. (B) Heat maps showing markers of different myeloid cell populations. (C) Dot plots showing markers of different myeloid cell populations. (D) The trajectory distribution of each myeloid cell population over time in different samples. On the right is the starting point of development and on the left is the developmental endpoint. (E) The ordering of myeloid cells along pseudotime in a two-dimensional state-space defined by Monocle 2. (F) The trajectory of three typical genes (APOC1, CD14, CD163).
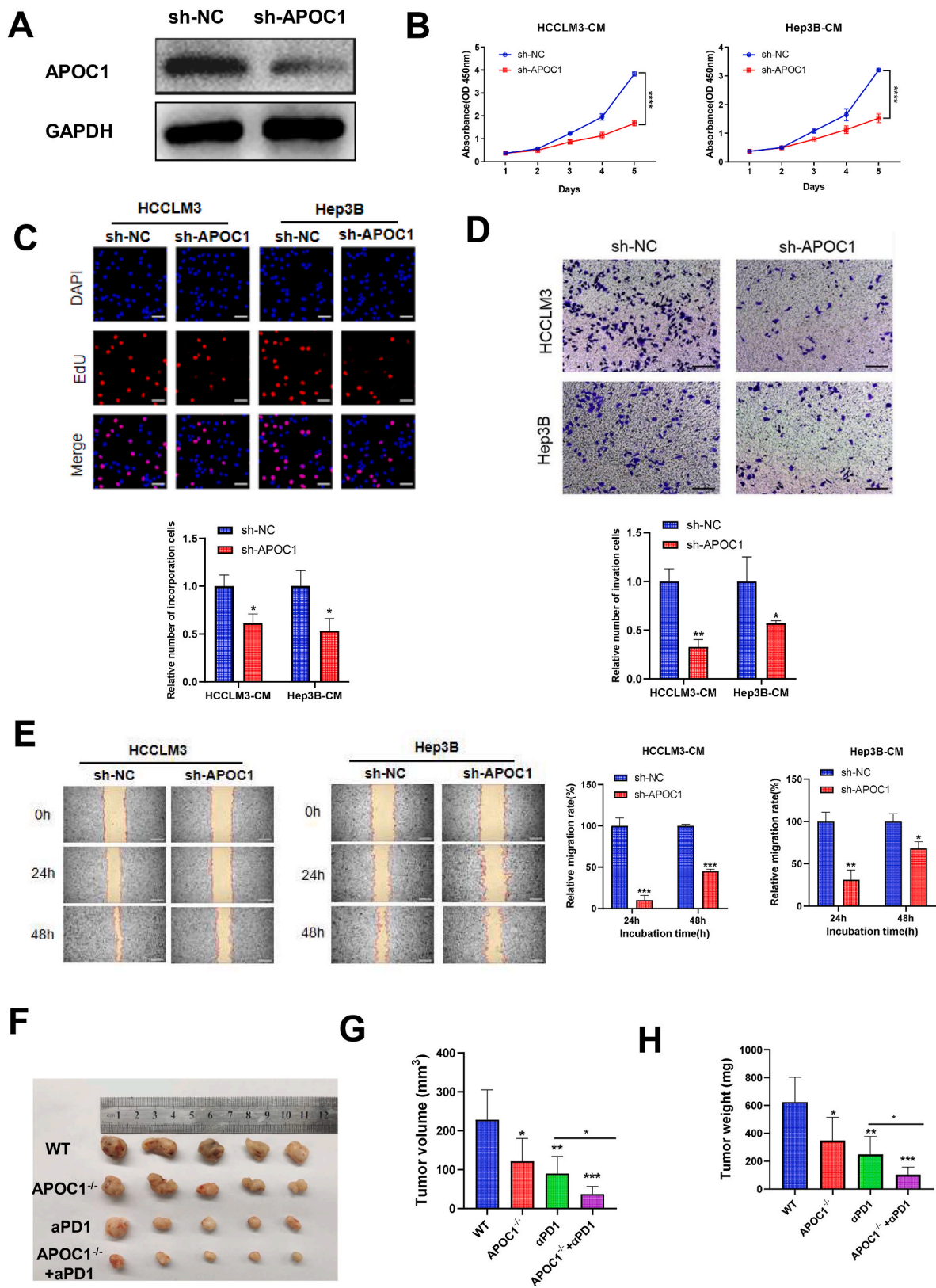
Fig. 4. Inhibition of APOC1 of TAM reduced HCC progression in vitro and in vivo.(A) Knockdown of APOC1 was demonstrated by Western blot in TAM cells.(B) CCK8 assay of HCC cancer cells with TAM supernatant in different groups.(C)EDU asasy of cancer cells with TAM supernatant in different groups.(D) Transwell assay of cancer cells with TAM supernatant in different groups.(E) Scratch assay of cancer cells with TAM supernatant in different groups.(F)Picture display of the respective group of subcutaneous tumors. (G–H) The volume (G) and weight (H) statistics of subcutaneous tumors in the respective group. *$p < 0.05$, **$p < 0.01$, ***$p < 0.001$.
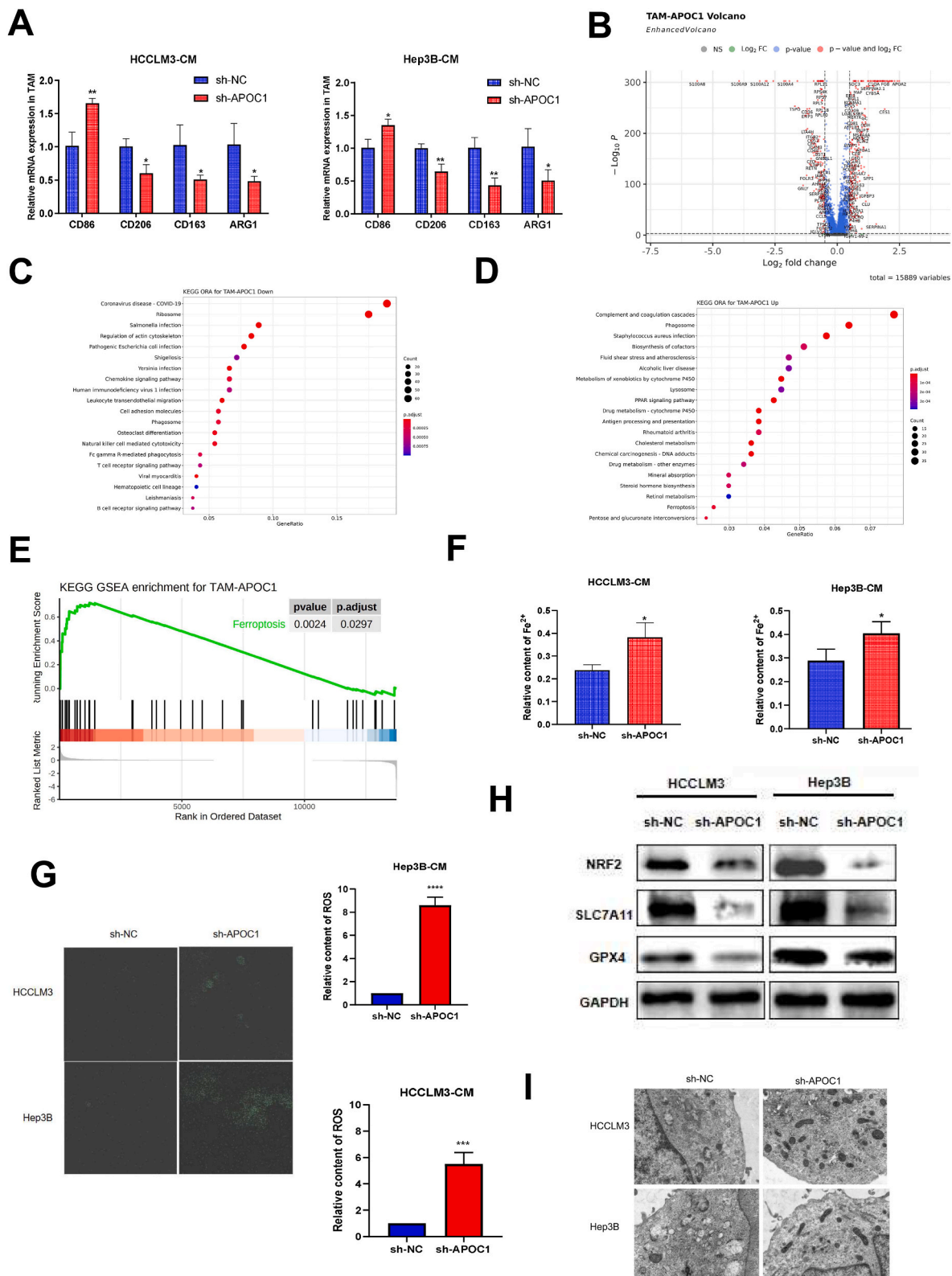
Fig. 5. Inhibition of APOC1 reversed the M2 phenotype to the M1 phenotype via the ferroptosis pathway in TAMs from HCC. (A) qRT-PCR results of M1/M2 phenotype gene expression in the sh-APOC1 and sh-NC group after of HCC cancer cell supernatant to TAM cells activation. (B)Volcano plot showing the differential genes in the TAM-APOC1 cell cluster.(C)KEGG plot showing pathway enrichment of differentially down-expressed genes in TAM-APOC1 cell cluster.(D)KEGG plot showing pathway enrichment of differentially up-expressed genes in TAM-APOC1 cell cluster.(E) GSEA enrichment of differential genes in the TAM-APOC1 cell cluster.(F)Iron content in sh-NC and sh-APOC1 groups of TAM cells.(G)ROS content in sh-NC and sh-APOC1 groups of TAM cells.(H)Ferroptosis-associated protein expression in sh-NC and sh-APOC1 groups of TAM cells.(I)Electron micrograph in sh-NC and sh-APOC1 groups of TAM cells. *$p < 0.05$, **$p < 0.01$, ***$p < 0.001$, ****$p < 0.0001$.

Because the expressions of PD-L1 and PD1 were up-regulated by APOC1 knockout in this study, we believed the combination of PD1 monoclonal antibody (mAb) could further suppress tumors in HCC. To confirm this idea, we injected H22 cells into WT and APOC1 $^{-/-}$ C57BL/6 mice subcutaneously and then conducted the PD1 mAb injection for seven days to assess their anti-tumor capability (Fig. 4F). The results demonstrated that, compared with the αPD1 group, the volume and weight of the tumor decreased significantly in the APOC1 $^{-/-}$ +αPD1 group (Fig. 4G–H). According to the immunohistochemistry results, the knockout of APOC1 caused the increase of CD3, CD8, PD1, and PD-L1, which is consistent with the results of mass spectrometry (Fig. 7A–C). Therefore, APOC1 deficiency resulted in immune activation and enhanced sensitivity to *anti*-PD1 therapy in HCC.

3.8. APOC1 was a marker to predict the sensitivity of anti-PD1 in HCC

To further analyze the findings' significance in human samples, we investigated APOC1, PD1, and PD-L1 protein expressions from five human HCC specimens using immunohistochemistry. As indicated from the correlation analysis, the expression of APOC1 demonstrated a negative correlation with PD1 and PD-L1 in carcinomas (Fig. 7D). Patients with high APOC1 expression seem to have low PD1 and PD-L1 expression (Fig. 7E). TISIDB database demonstrated that APOC1 expression was negatively correlated with PD1, PD-L1, TIGIT, and CD86 in 373 HCC samples (Figure S6), which was consistent with the mass spectrometry results of APOC1$^{-/-}$ mice. Altogether, APOC1 may act as a marker to predict the sensitivity of *anti*-PD1 in HCC.

4. Discussion

By sequencing at a single cell level, scRNA-seq solves the problem that the heterogeneity of different cells cannot be obtained from tissue samples, or the sample size is too small for routine sequencing, providing a new direction for scientists to study the behavior and mechanism of a single cell. The pathogenesis of HCC is still a difficult problem, and scRNA-seq can provide more in-depth research on the biological behavior of cells in the tumor microenvironment of HCC, especially by analyzing the cell population on a single cell basis [22]. In the present study, we performed deep scRNA-seq on the immune cell under the isolation in peripherally blood, cancer tissues, and nearby common tissues of four HCC cases and two non-cancer controls, and a total of 212,494 cells were included in the analysis. We identified distinct immune cell subtypes, enriched pathways for differential genes, and delineated associated developmentally relevant trajectories. In particular, we focused on analyzing myeloid cells and analyzed the different cell clusters of myeloid cells in detail. Pseudo-chronological analysis indicated that the middle and late stages of myeloid cell differentiation mainly included TAM-APOC1, TAM-CCL5, and TAM-FCN3 cell clusters were mainly enriched in tumor tissues. Mono-LST1 and Mono-S100A8 were enriched in the peripheral blood and were in the early stages of myeloid cell differentiation. Myeloid cells are abundant in the HCC tumor microenvironment and have been linked to uncontrolled malignant growth. Myeloid cells are generated from myeloid progenitors and immature myeloid cells, which terminally differentiate into mature granulocytes, monocytes/macrophages, and dendritic cells [23]. These cells function to phagocytize dying cells, eliminate foreign substances, repair tissue, and stimulate lymphocytes to respond to pathogens. In cancer patients, tumors globally alter the differentiation and function of myeloid cells, shifting them into immunosuppressive and tumor-promoting cells such as TAMs and Myeloid-derived suppressor cells (MDSCs). TAMs and MDSCs have been well recognized for their immunosuppressive function in HCC. Other functions of myeloid cells have also been documented, including the promotion of tumor incidence, invasion, metastasis, and angiogenesis [24]. A better understanding of myeloid cells in HCC will be crucial for developing effective HCC therapy.

Based on scRNA-seq results, we found that APOC1 was highly enriched in TAM cell cluster analysis. Different subgroup analyses of different samples suggested that the expression of APOC1 in the TAM cell cluster in HCC cancer tissues was significantly higher than that in adjacent cancer tissues. APOC1 is a polypeptide with 57 amino acid residues synthesized primarily in the liver and secreted into serum by autocrine. APOC1 genes are expressed primarily in the liver and the lungs, skin, testes, and spleen [25,26]. Recently, the relationship between APOC1 and cancer has been highlighted. However, most of the previous studies have focused on the relationship between APOC1 and tumor tissue, demonstrating the role of APOC1 in promoting tumor development by studying relevant signaling pathways or cytokines, and very few studies have focused on the TME. Therefore, in this study, we took a novel perspective, emphasizing the function of APOC1 in TAMs and thus influencing the TME of HCC. TAMs is one of the important members of TME, which can be divided into M1 macrophages and M2 macrophages. The gene expression patterns of TAMs and M2 macrophages are very different, and completely different gene regulation systems respectively control them. TAMs have an M1-like proinflammatory phenotype in the early stage of tumorigenesis and inhibit the immune response of tumor growth. As the tumor progresses, hypoxia of TME will gradually induce the M2-like transformation of TAMs and then promote them to participate in the immune escape and angiogenesis of tumor cells. There is abundant evidence that these two types of macrophages can transform into each other due to changes in TME. In this study, HCC cell supernatant was used to stimulate THP-1 cell, and the results demonstrated that the M1 marker was significantly higher in the sh-APOC1 group than in the control group, and the M2 marker was significantly lower in the sh-APOC1 group than in the control group. In addition, we stimulated HCC cells with TAM supernatant and found that TAMs in the sh-APOC1 group significantly reduced the proliferation, invasion, and migration of HCC cells than in the control group. All these findings suggest that APOC1 plays a crucial role in TAMs to promote HCC progression.

To investigate the mechanism by which the reduction of APOC1 leads to the transformation of TAMs from M2 to M1 phenotype, we analyzed the differential genes in the TAM-APOC1 cell population. KEGG and GSEA enrichment both confirmed that differentially expressed genes in the TAM-APOC1 cluster were involved in the ferroptosis pathway. Ferroptosis is a kind of programmed cell death newly discovered by Dixon in 2012, which exists in various diseases, such as kidney disease, liver disease, and nervous system disease [27,28]. The main mechanism of ferroptosis is to catalyze the lipid peroxidation of highly expressed unsaturated fatty acids on cell membranes under the action of iron divalent or ester oxygenase, which leads to cell death. In addition to iron metabolism, lipid metabolism and amino acid metabolism also play a role in ferroptosis; GPX4 and GSH regulate ROS levels through the NRF2 pathway. With the depletion of GPX4 or GSH, ROS accumulation in cells can directly lead to lipid peroxidation [29,30]. Iron overload and some cytokines released by iron-bearing cells have been demonstrated to affect the polarization and recruitment of macrophages during ferroptosis. As mentioned before, TAM phenotypes respond quickly to stimuli in specific environments and are transformed into each other between M1 and M2 types, and TAMs of the two phenotypes secrete different cytokines [31–33]. Research has confirmed that ROS impacts macrophage recruitment and polarization of an important factor, the role of ROS in polarization is very complex. In most cases, such as periodontitis, diabetes, cancer of the stomach, macrophages of ROS induce macrophages to M1, thereby increasing the release of inflammatory factors and form of promoting inflammatory TME [34]. In our experiments, Western blot, iron, and ROS detection confirmed that knockdown of APOC1 up-regulated ferroptosis and produced ROS through the pathways of iron metabolism and lipid metabolism, inducing the polarization of TAM into M1 type and inhibiting HCC.

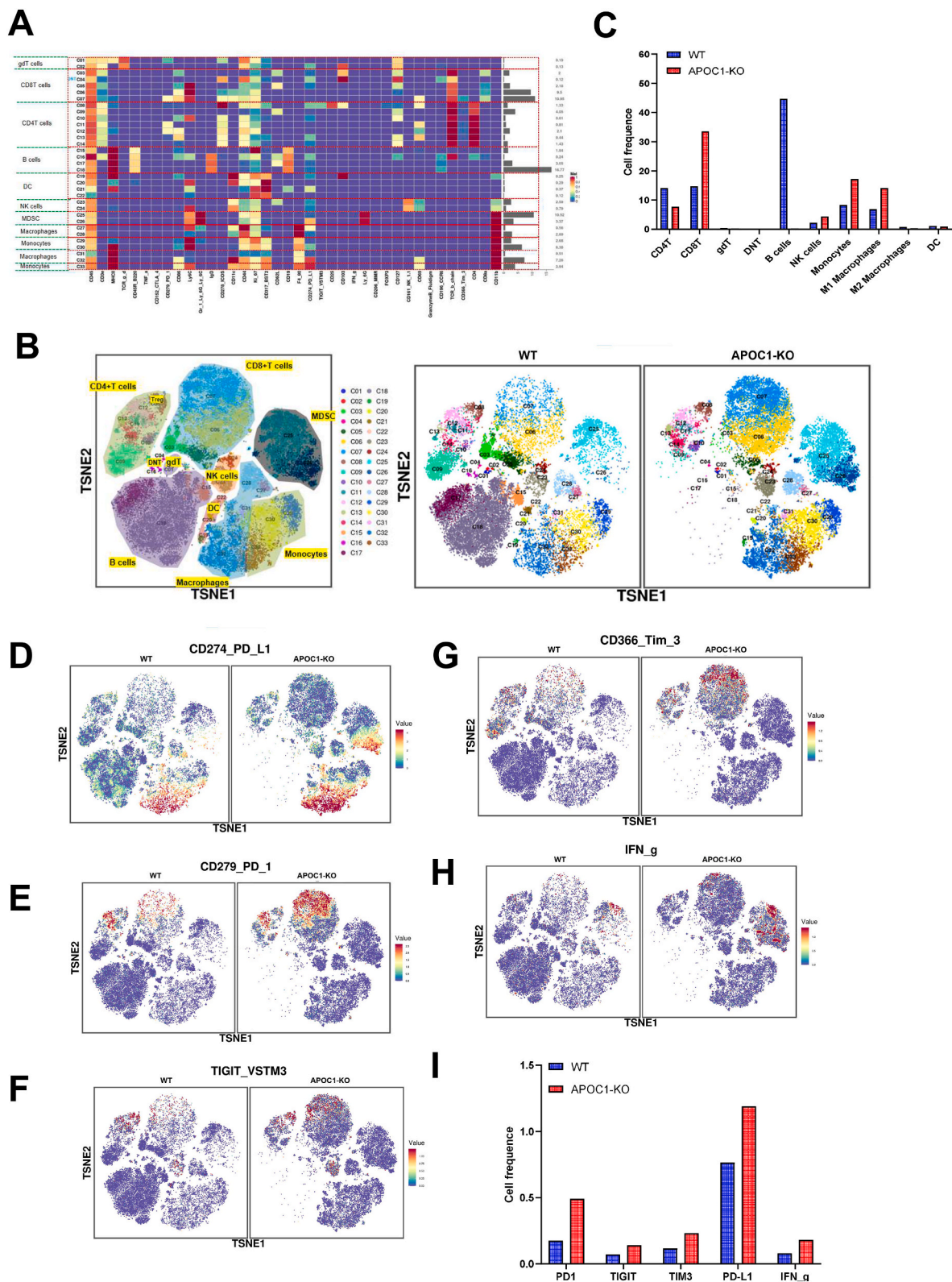Mass spectrometry can achieve precise immunophenotyping of cell

Fig. 6. APOC1 deficiency resulted in immune activation based on mass spectrometry analysis and enhanced sensitivity to *anti*-PD1 therapy in HCC. (A) A total of 33 cell clusters were divided, and we defined the respective cell cluster. (B) TSNE plot showing distributions of 33 cell clusters in the respective sample. (C) The histogram showing the number of the respective cell cluster in different groups. (D–H) TSNE plot showing the distribution of PD-L1, PD1, TIGIT, TIM3, IFNg in subcutaneous HCC tumors in different groups. (I) The histogram showing the number of PD-L1, PD1, TIGIT, TIM3, IFNg cells cluster in different groups.
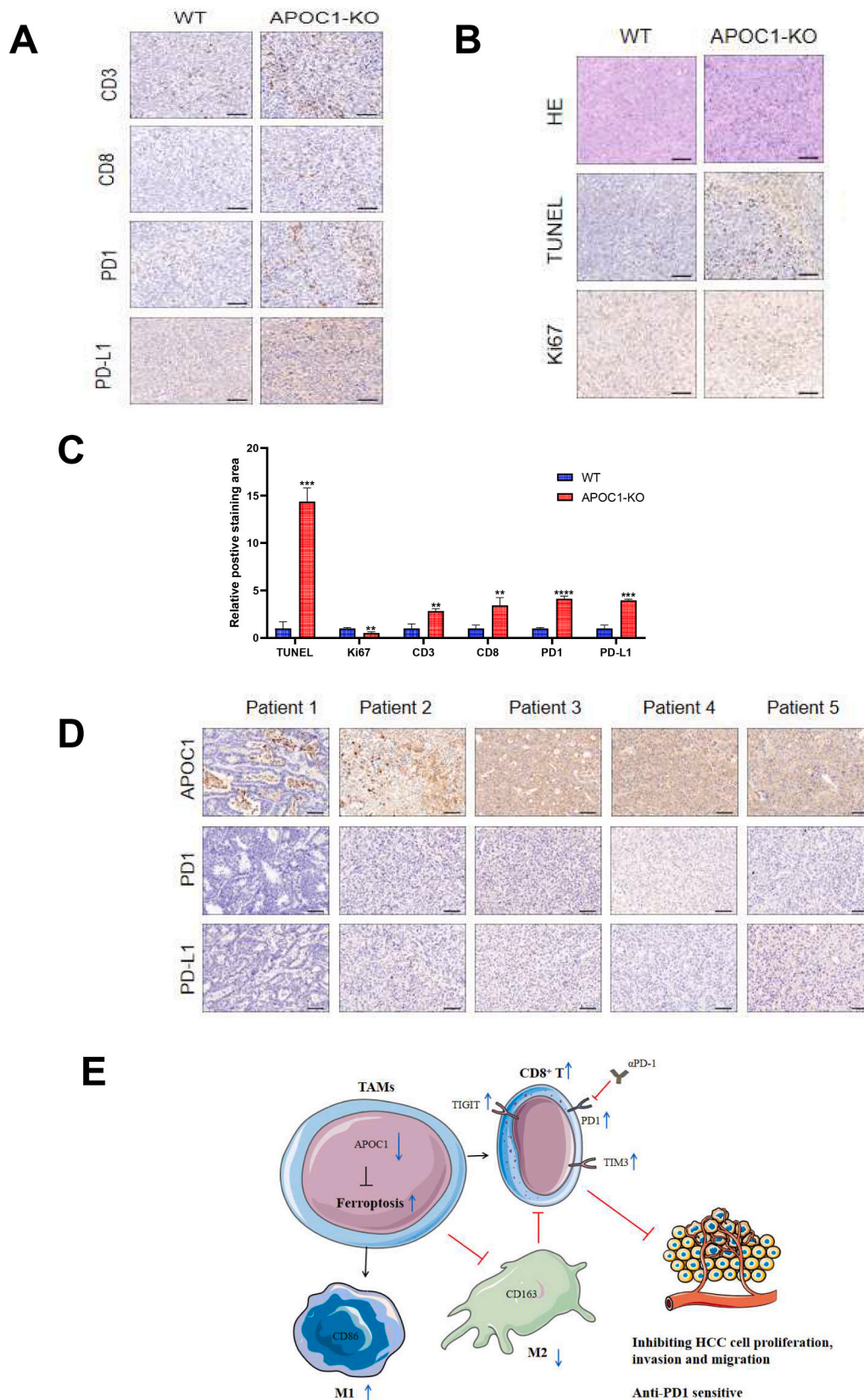
Fig. 7. APOC1 was a marker to predict the sensitivity of *anti*-PD1 in HCC. (A–B) The morphology of subcutaneous tumors in two groups was confirmed by HE staining. Immunohistochemical results of Ki67, TUNEL, PD-L1, CD3, and CD8 expression in the respective group was shown. (C)The panel illustrating the results of corresponding indicator statistics in two groups. (D)APOC1, PD1 and PD-L1 protein expressions from 5 human tumor specimens by using immunohistochemistry. (E) Mechanism schema diagram. Inhibition of APOC1 can promote the transformation of M2 macrophages into M1 macrophages through the ferroptosis pathway, thus reshaping the tumor immune microenvironment, especially enhancing the expression of CD8+T cells and enhancing the *anti*-PD1 immunotherapy for HCC. *p < 0.05, **p < 0.01, ***p < 0.001, ****p < 0.0001.

populations, comprehensive analysis of intracellular signaling networks, functional connections between cell subsets, and high-throughput multi-parameter detection of many samples. This study is the first to report changes in the immune microenvironment of HCC tumors in WT and APOC1$^{-/-}$ mice based on mass spectrometry. The results demonstrated that the relative proportions of CD8 T cells, M1 macrophages, and NK cells in APOC1$^{-/-}$ groups increased more than in the WT group. CD8 T cells specifically recognize and kill tumor cells by releasing cytotoxic molecules in the anti-tumor immune response, suggesting that the loss of APOC1 can trigger the activation of CD8$^+$ T cells and enhance tumor immunity [35]. Moreover, PD1/PD-L1 expression increased in APOC1$^{-/-}$ mice. We then injected H22 cells subcutaneously in WT and APOC1$^{-/-}$ mice, followed by PD1 mAb on day 7, and demonstrated a significant reduction in tumor volume and weight in the APOC1$^{-/-}$+αPD1 group than in the αPD1 group. Therefore, knockdown of APOC1 significantly enhanced the therapeutic efficacy of PD1 mab in HCC. Although drugs targeting the PD1/PD-L1 immune checkpoint have antitumor activity in HCC patients, response rates are generally low (20%–40%) [36,37]. In addition, PD1/PD-L1 mAb must be combined with other drugs to enhance efficacy, leading to excessive drug toxicity. Approximately 59% of patients had to stop this immunotherapy because of severe immune-related adverse events (irAEs) [38]. Therefore, not all patients can obtain clinical benefits from PD1 or PD-L1 checkpoint blocking therapy and enhancing the reactivity of PD1/PD-L1 mAb will have important clinical significance.

5. Conclusion

In summary, the present study revealed that inhibition of APOC1 can promote the transformation of M2 macrophages into M1 macrophages via the ferroptosis pathway, thereby reshaping the tumor immune microenvironment and improving the *anti*-PD1 immunotherapy for HCC, providing a new strategy for improving the therapeutic effect of *anti*-PD1, and bringing new hope to HCC patients (Fig. 7E).

Authors' contributions

There are 4 first authors in this manuscript and they have equally contributed to this project. Dr. XPH, ZYZ, HYL and YZ were responsible for designing and performing the experiments. Dr. JWK, XYK, DWR, GSS, and GQS contributed to performing part of experiment. Furthermore, we have 4 corresponding authors in this manuscript. Dr. HBY, LL, WWT and XHW have contributed to data interpretation, editing and critical revision of the manuscript. XHW and WWT have contributed to study design and critical revision of the manuscript. All authors read and approved the final manuscript.

Declaration of competing interest

The authors declare that they have no competing interests.

Data availability

All relevant data are provided in the paper and supporting information file.

Appendix A. Supplementary data

Supplementary data related to this article can be found at https://doi.org/10.1016/j.redox.2022.102463.

References

[1] H. Sung, J. Ferlay, R.L. Siegel, M. Laversanne, I. Soerjomataram, A. Jemal, et al., Global cancer statistics 2020: GLOBOCAN estimates of incidence and mortality worldwide for 36 cancers in 185 countries, CA A Cancer J. Clin. 71 (2021) 209–249.

[2] T. Clark, S. Maximin, J. Meier, S. Pokharel, P. Bhargava, Hepatocellular carcinoma: review of epidemiology, screening, imaging diagnosis, response assessment, and treatment, Curr. Probl. Diagn. Radiol. 44 (2015) 479–486.

[3] J. Han, B. Wang, W. Liu, S. Wang, R. Chen, M. Chen, et al., Declining disease burden of hepatocellular carcinoma in the US, 1992-2017: a population-based analysis, Hepatology 76 (2022) 576–588.

[4] A.-L. Cheng, Y.-K. Kang, Z. Chen, C.-J. Tsao, S. Qin, J.S. Kim, et al., Efficacy and safety of sorafenib in patients in the Asia-Pacific region with advanced hepatocellular carcinoma: a phase III randomised, double-blind, placebo-controlled trial, Lancet Oncol. 10 (2009) 25–34.

[5] U. Harkus, M. Wankell, P. Palamuthusingam, C. McFarlane, L. Hebbard, Immune checkpoint inhibitors in HCC: cellular, molecular and systemic data, in: Seminars in Cancer Biology, Elsevier, 2022, 2022.

[6] D.M. Pardoll, The blockade of immune checkpoints in cancer immunotherapy, Nat. Rev. Cancer 12 (2012) 252–264.

[7] M. Ringelhan, D. Pfister, T. O'Connor, E. Pikarsky, M. Heikenwalder, The immunology of hepatocellular carcinoma, Nat. Immunol. 19 (2018) 222–232.

[8] A.B. El-Khoueiry, B. Sangro, T. Yau, T.S. Crocenzi, M. Kudo, C. Hsu, et al., Nivolumab in patients with advanced hepatocellular carcinoma (CheckMate 040): an open-label, non-comparative, phase 1/2 dose escalation and expansion trial, Lancet 389 (2017) 2492–2502.

[9] T. Yau, J.-W. Park, R.S. Finn, A.-L. Cheng, P. Mathurin, J. Edeline, et al., Nivolumab versus sorafenib in advanced hepatocellular carcinoma (CheckMate 459): a randomised, multicentre, open-label, phase 3 trial, Lancet Oncol. 23 (2022) 77–90.

[10] R.S. Finn, S. Qin, M. Ikeda, P.R. Galle, M. Ducreux, T.-Y. Kim, et al., Atezolizumab plus bevacizumab in unresectable hepatocellular carcinoma, N. Engl. J. Med. 382 (2020) 1894–1905.

[11] F. Tang, C. Barbacioru, Y. Wang, E. Nordman, C. Lee, N. Xu, et al., mRNA-Seq whole-transcriptome analysis of a single cell, Nat. Methods 6 (2009) 377–382.

[12] S. Borgquist, T. Butt, P. Almgren, D. Shiffman, T. Stocks, M. Orho-Melander, et al., Apolipoproteins, lipids and risk of cancer, Int. J. Cancer 138 (2016) 2648–2656.

[13] J. Yi, L. Ren, J. Wu, W. Li, X. Zheng, G. Du, et al., Apolipoprotein C1 (APOC1) as a novel diagnostic and prognostic biomarker for gastric cancer, Ann. Transl. Med. 7 (2019).

[14] H.L. Ko, Y.S. Wang, W.L. Fong, M.S. Chi, K.H. Chi, S.J. Kao, Apolipoprotein c1 (apoc 1) as a novel diagnostic and prognostic biomarker for lung cancer: a marker phase i trial, Thoracic cancer 5 (2014) 500–508.

[15] H. Ren, Z. Chen, L. Yang, W. Xiong, H. Yang, K. Xu, et al., Apolipoprotein C1 (APOC1) promotes tumor progression via MAPK signaling pathways in colorectal cancer, Cancer Manag. Res. 11 (2019) 4917.

[16] Wp Su, Ln Sun, Sl Yang, H. Zhao, Ty Zeng, Wz Wu, et al., Apolipoprotein C1 promotes prostate cancer cell proliferation in vitro, J. Biochem. Mol. Toxicol. 32 (2018), e22158.

[17] Y-l Li, L-w Wu, L-h Zeng, Z-y Zhang, W. Wang, C. Zhang, et al., ApoC1 promotes the metastasis of clear cell renal cell carcinoma via activation of STAT3, Oncogene 39 (2020) 6203–6217.

[18] P. Handa, S. Thomas, V. Morgan-Stevenson, B.D. Maliken, E. Gochanour, S. Boukhar, et al., Iron alters macrophage polarization status and leads to steatohepatitis and fibrogenesis, J. Leukoc. Biol. 105 (2019) 1015–1026.

[19] X. Hu, X. Cai, R. Ma, W. Fu, C. Zhang, X. Du, Iron-load exacerbates the severity of atherosclerosis via inducing inflammation and enhancing the glycolysis in macrophages, J. Cell. Physiol. 234 (2019) 18792–18800.

[20] Y. Zhou, K.T. Que, Z. Zhang, Z.J. Yi, P.X. Zhao, Y. You, et al., Iron overloaded polarizes macrophage to proinflammation phenotype through ROS/acetyl-p53 pathway, Cancer Med. 7 (2018) 4012–4022.

[21] J.-K. Kao, S.-C. Wang, L.-W. Ho, S.-W. Huang, C.-H. Lee, M.-S. Lee, et al., M2-like polarization of THP-1 monocyte-derived macrophages under chronic iron overload, Ann. Hematol. 99 (2020) 431–441.

[22] L. Li, L. Shen, J. Ma, Q. Zhou, M. Li, H. Wu, et al., Evaluating distribution and prognostic value of new tumor-infiltrating lymphocytes in HCC based on a scRNA-Seq study with CIBERSORTx, Front. Med. 7 (2020) 451.

[23] E. Zhao, H. Xu, L. Wang, I. Kryczek, K. Wu, Y. Hu, et al., Bone marrow and the control of immunity, Cell. Mol. Immunol. 9 (2012) 11–19.

[24] S. Wan, N. Kuo, I. Kryczek, W. Zou, T.H. Welling, Myeloid cells in hepatocellular carcinoma, Hepatology 62 (2015) 1304–1312.

[25] J.F. Berbée, C.C. van der Hoogt, R. Kleemann, E.F. Schippers, R.L. Kitchens, J. T. van Dissel, et al., Apolipoprotein CI stimulates the response to lipopolysaccharide and reduces mortality in Gram-negative sepsis, Faseb. J. 20 (2006) 2162–2164.

[26] S. Takano, H. Yoshitomi, A. Togawa, K. Sogawa, T. Shida, F. Kimura, et al., Apolipoprotein C-1 maintains cell survival by preventing from apoptosis in pancreatic cancer cells, Oncogene 27 (2008) 2810–2822.

[27] K. Yang, H. Song, D. Yin, PDSS2 inhibits the ferroptosis of vascular endothelial cells in atherosclerosis by activating Nrf2, J. Cardiovasc. Pharmacol. 77 (2021) 767.

[28] D. Ma, C. Li, P. Jiang, Y. Jiang, J. Wang, D. Zhang, Inhibition of ferroptosis attenuates acute kidney injury in rats with severe acute pancreatitis, Dig. Dis. Sci. 66 (2021) 483–492.

[29] L. Wang, Y. Liu, T. Du, H. Yang, L. Lei, M. Guo, et al., ATF3 promotes erastin-induced ferroptosis by suppressing system Xc, Cell Death Differ. 27 (2020) 662–675.

[30] C. Guo, P. Liu, G. Deng, Y. Han, Y. Chen, C. Cai, et al., Honokiol induces ferroptosis in colon cancer cells by regulating GPX4 activity, Am J. Cancer Res. 11 (2021) 3039.

[31] Y. Yuan, Y. Chen, T. Peng, L. Li, W. Zhu, F. Liu, et al., Mitochondrial ROS-induced lysosomal dysfunction impairs autophagic flux and contributes to M1 macrophage polarization in a diabetic condition, Clin. Sci. 133 (2019) 1759–1777.

[32] A.P. West, I.E. Brodsky, C. Rahner, D.K. Woo, H. Erdjument-Bromage, P. Tempst, et al., TLR signalling augments macrophage bactericidal activity through mitochondrial ROS, Nature 472 (2011) 476–480.

[33] W. Aerbajinai, M.C. Ghosh, J. Liu, C. Kumkhaek, J. Zhu, K. Chin, et al., Glia maturation factor-γ regulates murine macrophage iron metabolism and M2 polarization through mitochondrial ROS, Blood Adv. 3 (2019) 1211–1225.

[34] B. Zhang, Y. Yang, J. Yi, Z. Zhao, R. Ye, Hyperglycemia modulates M1/M2 macrophage polarization via reactive oxygen species overproduction in ligature-induced periodontitis, J. Periodontal. Res. 56 (2021) 991–1005.

[35] A. Gabrielson, Y. Wu, H. Wang, J. Jiang, B. Kallakury, Z. Gatalica, et al., Intratumoral CD3 and CD8 T-cell densities associated with relapse-free survival in HCC, Cancer Immunol. Res. 4 (2016) 419–430.

[36] M. Pinter, R.K. Jain, D.G. Duda, The current landscape of immune checkpoint blockade in hepatocellular carcinoma: a review, JAMA Oncol. 7 (2021) 113–123.

[37] O. Hamid, C. Robert, A. Daud, F. Hodi, W. Hwu, R. Kefford, et al., Five-year survival outcomes for patients with advanced melanoma treated with pembrolizumab in KEYNOTE-001, Ann. Oncol. 30 (2019) 582–588.

[38] A.M. Luoma, S. Suo, H.L. Williams, T. Sharova, K. Sullivan, M. Manos, et al., Molecular pathways of colon inflammation induced by cancer immunotherapy, Cell 182 (2020) 655–671, e622.